mathematics

MDPI

Article

Multiscale 1D-CNN for Damage Severity Classification and Localization Based on Lamb Wave in Laminated Composites

Olivier Munyaneza [1] and Jung Woo Sohn [2,*]

[1] Department of Aeronautics, Mechanical and Electronic Convergence Engineering, Graduated School, Kumoh National Institute of Technology, Daehak-ro 61, Gumi 39177, Gyeongbuk, Republic of Korea; olivis@kumoh.ac.kr

[2] School of Mechanical System Engineering, Kumoh National Institute of Technology, Daehak-ro 61, Gumi 39177, Gyeongbuk, Republic of Korea

* Correspondence: jwsohn@kumoh.ac.kr

Abstract: Lamb-wave-based structural health monitoring is widely employed to detect and localize damage in composite plates; however, interpreting Lamb wave signals remains challenging due to their dispersive characteristics. Although convolutional neural networks (CNNs) demonstrate a significant capability for pattern recognition within these signals relative to other machine learning models, CNNs frequently encounter difficulties in capturing all the underlying patterns when the damage severity varies. To address this issue, we propose a multiscale, one-dimensional convolutional neural network (MS-1D-CNN) to assess the damage severity and localize damage in laminated plates. The MS-1D-CNN is capable of learning both low- and high-level features, enabling it to distinguish between minor and severe damage. The dataset was obtained experimentally via a sparse array of four lead zirconate titanates, with signals from twelve paths fused and downsampled before being input into the model. The efficiency of the model was evaluated using accuracy, precision, recall, and F1-score metrics for severity identification, along with the mean squared error, mean absolute error, and R^2 for damage localization. The experimental results indicated that the proposed MS-1D-CNN outperformed support vector machine and artificial neural network models, achieving higher accuracy in both identifying damage severity and localizing damage with minimal error.

Keywords: lamb wave; damage classification; damage localization; multiscale 1D-CNN; artificial neural networks (ANNs); support vector machine (SVM); fully convolutional networks (FCNs)

MSC: 68T01

check for updates

Academic Editor: Jinwoo Song

Received: 29 December 2024
Revised: 22 January 2025
Accepted: 23 January 2025
Published: 25 January 2025

Citation: Munyaneza, O.; Sohn, J.W. Multiscale 1D-CNN for Damage Severity Classification and Localization Based on Lamb Wave in Laminated Composites. *Mathematics* **2025**, *13*, 398. https://doi.org/10.3390/math13030398

Copyright: © 2025 by the authors. Licensee MDPI, Basel, Switzerland. This article is an open access article distributed under the terms and conditions of the Creative Commons Attribution (CC BY) license (https://creativecommons.org/licenses/by/4.0/).

1. Introduction

Recently, composite materials have gained popularity due to their superior properties over metals, such as high strength, durability, corrosion resistance, lightweight, and customizable characteristics [1,2], which make them suitable for various engineering fields, including aircraft, automobile, renewable energy, sports products, and construction [3–5]. However, the heterogeneous and anisotropic nature of composite materials makes them susceptible to different types of damage, such as delamination, matrix cracking, and other inherent damages [6,7]. Therefore, an effective approach to detect and localize damage at the initial stage is crucial for ensuring the safety and integrity of the structure.

To monitor the initiation and progression of damage, structural health monitoring (SHM) and nondestructive evaluation (NDE) techniques have been developed over the

last few decades to detect small defects and ensure the safe operation of composite structures [8,9]. The SHM technique employs permanent sensors bonded to a structure with the ability to excite, collect, analyze, and interpret data to predict the current status of the structure through physics or data-driven techniques [10]. Lamb waves are widely used in SHM techniques for detecting and localizing damage in composite structures. Lamb waves are elastic waves capable of propagating through thin-plate structures. These waves are widely used due to their various benefits, such as high sensitivity to smaller defects, long travel distances with small attenuation, and the ability to monitor larger areas with sparse piezoelectric sensors [11–13]. Numerous studies have reported the detection and localization of damage based on Lamb waves. Carlos et al. [14] proposed a damage-localization imaging algorithm for detecting delamination in a quasi-isotropic laminate using a transducer network to scan the entire structure to detect damage through the nonlinear response of Lamb waves. Zeng et al. [15] proposed an innovative damage location identification and size quantification assessment method based on the Lamb wave and a weighted average imaging algorithm, together with a scaling factor. Yang et al. [16] proposed an effective and practical tool for identifying damage in large plate structures. They developed a novel baseline-free damage approach that combines single-Lamb-wave mode extraction with phased array SHM. All the above-stated Lamb wave models are based on the physical behavior of the structure to detect undelayed changes in the properties or structural geometry of the structure. However, monitoring a structure based on a physical model presents several challenges, such as a lack of theoretical models, insufficient experimental observations, limited knowledge about the materials and loading conditions of the structure, and a lack of adaptability to unknown and complex damages [17–19]. The limitations of physics-based modeling have led to a shift toward data-driven approaches for SHM.

Data-driven approaches have proven to be more robust than physics-based models because they focus on learning data patterns using machine learning and deep learning techniques. Traditional machine learning methods, such as artificial neural networks, support vector machines (SVMs), K-nearest neighbors, and random forests, have been used to detect and localize damage in composite structures [20–22]. Viotti et al. [23] applied various machine learning methods to detect and identify damage in sandwich structures and employed an artificial neural network to localize and quantify the damage. They trained the models using simulated datasets and validated their performance with experimental datasets. Of the more than ten models, only the light-gradient boosting machine achieved an accuracy of 85%. In contrast, the artificial neural network (ANN) excelled in localizing the damages but struggled to estimate their size. Lim et al. [24] proposed an alternative strategy to predict and localize delamination in composite plates using a combination of random forest and natural frequency-shift damage. The proposed approach was capable of localizing damage with a correlation coefficient of 0.996 and an accuracy score of approximately 90% for classifying delamination. We employed and evaluated SVM, extra tree, gradient boost, AdaBoost, and decision tree approaches to improve the prediction of delamination in aircraft structures [25]. The best performance was obtained from the ensemble model, with a goodness of fit (R^2) of 0.975 and a 0.023 root mean squared error (RMSE) for the old coupon and an R^2 of 0.928 and a 0.053 RMSE for the new coupon. Gao et al. [26] proposed a damage localization method based on Lamb waves and a modular artificial neural network (M-ANN) to address the challenges faced by a data-driven approach in achieving precise damage localization. Many researchers have employed traditional machine learning in SHM to date. However, the complexity of Lamb wave signals and varying environmental factors, such as noise, humidity, and temperature, have presented challenges for these machine learning methods in classifying

damage despite their proficiency in pinpointing the location of the damage. Consequently, conventional machine learning techniques cannot deliver reliable damage monitoring when faced with complex datasets.

Deep learning has gained considerable attention in SHM for its ability to extract features from large, complex datasets and to localize and quantify damage in composite materials. Migot et al. [27] presented an automated system based on convolutional neural networks (CNNs) that is qualified to distinguish between damaged and pristine structures with three different classes. Lee et al. [28] investigated damage severity identification and localization using four distinct convolutional neural networks. Rosafalco et al. [29] proposed a novel approach for real-time structural health monitoring to detect and localize the damages through fully convolutional networks (FCNs).

The majority of deep learning frameworks rely on supervised learning, which requires a significant amount of time to label data as either healthy or damaged. Parziale et al. [30] proposed a framework that used conditional generative adversarial networks (CGANs) with convolutional layers for damage localization in composite plates—the model was trained only on a healthy dataset. The same unsupervised approach for classifying and localizing damage was used in [31–33]. The majority of damage-detection methods in SHM depend on 2D-CNNs, which transform the gathered Lamb waves into images prior to their input into a CNN. However, the high computational cost of 2D-CNNs limited their implementation in real-time SHM. To mitigate this issue, Afshin et al. [34] proposed a 1D-CNN to localize and characterize damage at three different levels. Zong et al. [35] proposed singular value decomposition for extracting features and used a 1D-CNN to train a model for detecting and localizing damage. The aforementioned 1D-CNN models have demonstrated their ability to automatically and efficiently extract critical features from one-dimensional Lamb wave signals, making them highly effective for damage detection and localization. However, traditional 1D-CNN architectures primarily focus on extracting temporal features from Lamb wave signals, which may limit their ability to fully capture the spatial characteristics associated with wave distortions caused by various types of damage and surrounding noise.

To address this issue, multiscale CNNs were designed to extract features at multiple scales from time-series signals. Fu et al. [36] introduced a deep CNN incorporating multiscale convolutional kernels in its first layer to improve the accuracy of fault diagnosis in rolling bearings. Using kernels of varying sizes, the model effectively captured features across multiple scales, enabling the detection of both subtle and significant fault characteristics in rolling-bearing signals. Li et al. [37] presented an end-to-end adaptive multiscale fully convolutional network for intelligent bearing fault diagnosis under various noise conditions. This model could adjust to different levels of noise and correctly extract fault-related features. To minimize the interference from sensing paths that carry less significant features and enhance the diagnostic performance of the model, Liao et al. [38] introduced dual MS-1D-CNNs. This innovative model can autonomously prioritize sensing paths that contain critical damage information while disregarding paths with limited or irrelevant data.

Inspired by References [35–37], an MS-1D-CNN for damage severity classification and localization is proposed in this paper. Unlike traditional 1D-CNNs, our framework incorporates multiscale convolutional layers that employ both small and large kernels to capture temporal and spatial features from raw Lamb wave signals simultaneously. This approach enhances the ability of the model to extract intricate patterns from signals, enabling precise and efficient damage detection. By directly processing raw Lamb wave data without converting them into 2D representations, our MS-1D-CNN reduces the computational overhead, making it a viable solution for real-time SHM applications. Furthermore, the

multiscale architecture improves the robustness and adaptability of the framework, thereby addressing the challenges posed by complex and noisy datasets in composite structures.

2. Proposed Methodology

The process of identifying and localizing damage consisted of four main steps in laminated composite materials, as shown in Figure 1. These included data acquisition, data preprocessing, the proposed multiscale 1D-CNN model, and final results. Four piezoelectric transducers were bonded to a manufactured composite plate during data acquisition to excite and collect Lamb waves. We simulated the damage severity in a composite plate using three different masses and collected three damage datasets. Moreover, the pristine composite plate provided health data. We processed the obtained guided wave in the second step to increase the sensitivity of damage detection, fused the signals from 12 paths into a single signal, and performed a downsampling process to mitigate the computational complexity. The third step was the multiscale 1D-CNN model, which aimed to extract features, train, and optimize. Moreover, we used the trained MS-1D-CNN model to classify and localize damage in the composite plates. Finally, we evaluated the results using various metrics, including accuracy, precision, recall, and F1-score for damage severity, and mean squared error, mean absolute error, and R^2 for damage localization.

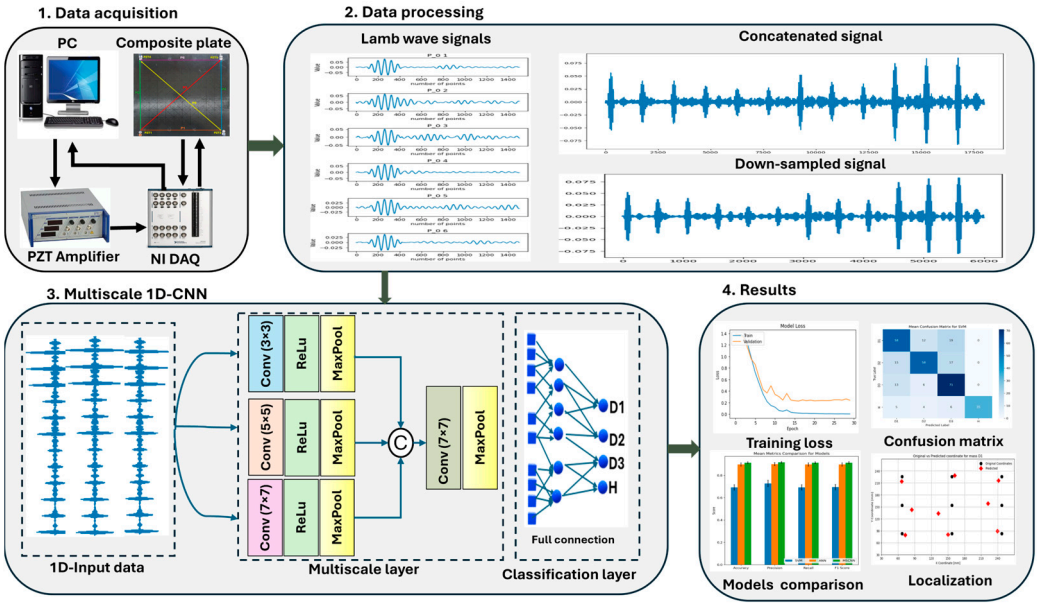


Figure 1. The proposed framework of MS-1D-CNN.

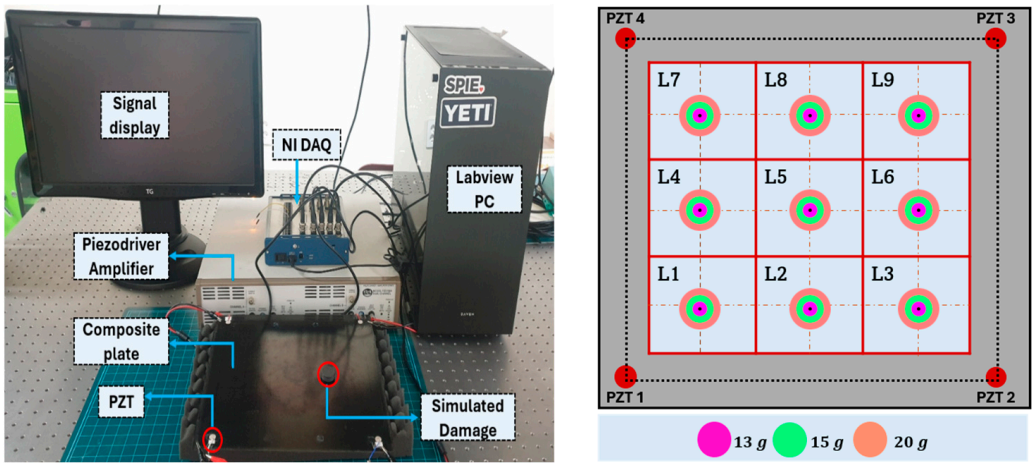
2.1. Material Preparation

The composite plates were fabricated using a hot-pressing machine by stacking eight plies of 320 × 320 mm carbon fiber prepregs (T700SC-12k-60E). The properties of the prepregs provided by the manufacturer included a tensile strength of 4900 Mpa, a tensile modulus of 230 GPa, a thermal conductivity of 9.4 W/m.K, density of 1.8 g/cm^3, elongation of 2.1%, and filament diameter of 7μ. The layups of the composite plate were arranged symmetrically with a stacking sequence of $[0°/0°]_{4s}$ cross-plies. After curing, a waterjet cutting machine was used to trim the composite plate, and the dimensions were reduced to 300 × 300 × 1 mm.

2.2. Lamb Wave Signal Acquisition

The guided-wave technique was used to investigate the delamination process in the composite plate, as shown in the experimental setup in Figure 2a. The setup comprised

a composite plate and a personal computer (PC) to generate Lamb waves and store data. A monitor was used for displaying Lamb wave signals. A NI USB-6341 data acquisition system transmitted the tone burst to excite the lead zirconate titanate (PZT) transducers and operate the working sequence of all PZT pairs. The input voltage applied to the PZT was enhanced by using a piezo-driver amplifier. The PZTs used were made from a PI ceramic (PRYY+0110), with a diameter of 10 mm and a thickness of 0.5 mm. The sensor array formed by four piezoelectric transducers, PZT1–PZT4, was glued to a composite plate using a Loctite 401 adhesive, and they were responsible for exciting and collecting Lamb wave signals.



(**a**) (**b**)

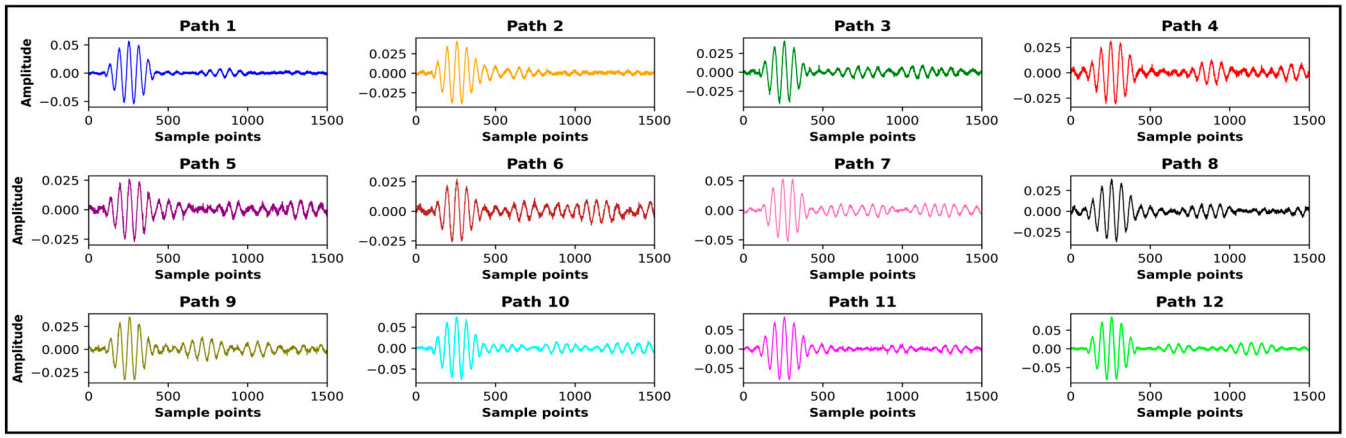
Figure 2. Experimental setup: (**a**) Lamb wave experimental setup and (**b**) damage location with three model defects.

In each experiment, each actuator–sensor pair was excited in the array in a round-robin fashion $n(n-1)$, acquiring a total of 12 distinct signals. To simulate the damage severity, three different masses of 13 g, 15 g, and 20 g, each with a uniform diameter of 24 mm, were positioned at designated locations on the composite plate. In the experiment, a 5-cycle Hanning tone burst with a central frequency of 150 kHz was employed to activate the PZT transducers. Lamb wave signals were acquired at a sampling rate of 500 kHz, using an excitation voltage of 50 V after amplification. For damage localization, the 270 × 270 mm square was subdivided into nine equal squares, as illustrated in Figure 2b. The mass blocks were sequentially positioned at the center of each square to simulate damage, with only one mass block placed on the plate during each experiment. A mass of 13 g was initially positioned at the target point to capture signals corresponding to damage severity D1. Following the initial recording, the first mass was substituted with 15 g to record the damage severity D2. Subsequently, the 15 g mass was replaced with a 20 g mass to record the damage severity D3. This procedure was repeated for all target locations. To ensure experimental repeatability, the signal acquisition was repeated 10 times, yielding 3240 damaged signals (12 paths × 10 repetitions × 9 locations × 3 masses) and 360 healthy signals (12 paths × 30 repetitions).

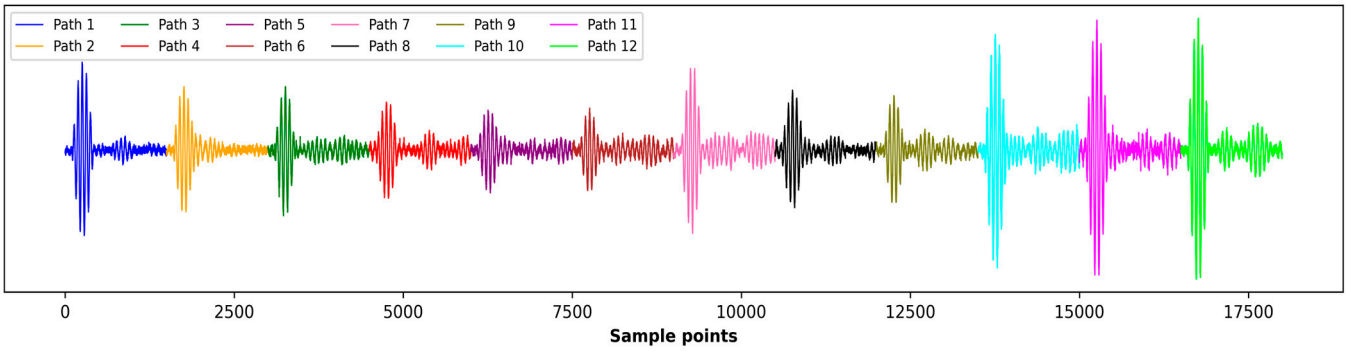
2.3. Data Preprocessing

The Lamb wave signals acquired in the experiment were processed to reduce the inherent complexity of the dataset. Initially, specific signals exhibited temporal patterns attributable to various factors, including PZT degradation, inadequate bonding between the sensor and composite plate, and improper fitting between the BNC cables and the tested plate. A detrending approach was employed for all raw Lamb wave data to mitigate

these patterns. Figure 3a presents the detrended Lamb wave signals for 12 paths obtained from a damage severity D1 of the 13 g mass placed at the coordinates (67 mm, 83 mm). The detrended Lamb waves from the 12 paths were fused to create a single signal, as shown in Figure 3b. This process enhanced the sensitivity to various damages and offered a more comprehensive assessment of structural conditions [39]. After the fusion process, we reduced the number of damaged signals from 3240 to 270 and fused the 360 health data signals into 30 signals, each containing 18,000 data points. A downsampling process was conducted to decrease the number of sampling points, facilitate faster computation, and remove redundant information from the signal. Consequently, the fused signals containing 18,000 data points were downsampled to 6000 data points, as shown in Figure 3c. To augment the sample size, Gaussian noise with a mean of zero and five standard deviations of 1%, 3%, 5%, 7%, and 9% were added to the downsampled signals. Incorporating Gaussian noise during augmentation introduced variability in the dataset, thereby enhancing the generalization capacity and robustness of the trained model. Typically, larger datasets are generally divided in a ratio of 80:20, whereas smaller datasets are frequently partitioned in a 70:30 ratio. In this study, 1600 signals were split into 70% for training and 30% for testing. We implemented the K-fold cross-validation method with five folds to balance the computational efficiency and reliable estimations, thereby minimizing the risk of overfitting and model bias.

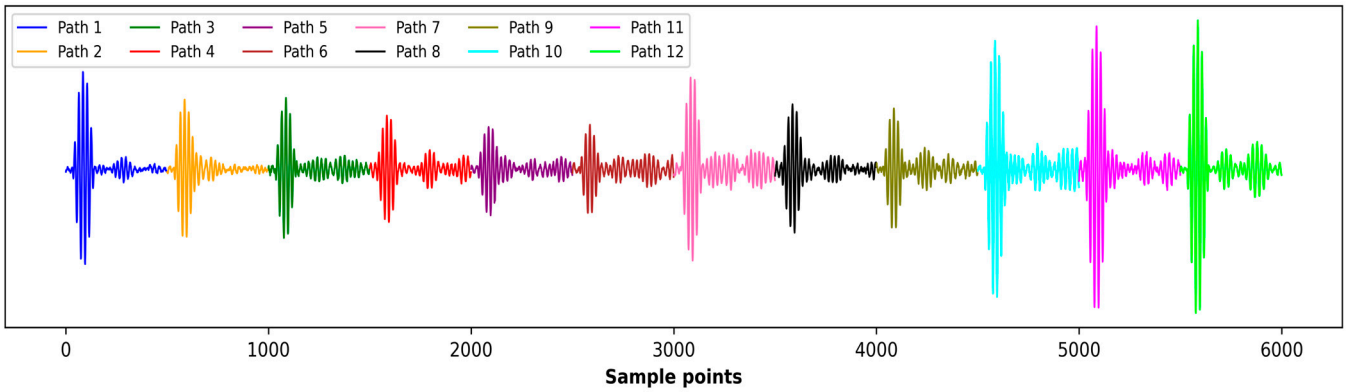


(**a**)



(**b**)

Figure 3. *Cont.*



(**c**)

Figure 3. Measured Lamb wave signals: (**a**) Lamb wave signals from 12 paths corresponding to damage severity (D1), located at coordinates (67, 83), (**b**) all 12 concatenated paths, and (**c**) downsampled signal.

2.4. ANNs

ANNs are computational models consisting of artificial neurons that can autonomously extract information from data. ANNs are well known for their learning and generalization capabilities, as well as their error tolerance [40]. The artificial neural network architecture established in this study had 1 input layer with 6000 features, 3 hidden layers with multiple neurons, and 1 output layer representing 3 damage severities ($D1$, $D2$, and $D3$) and 1 intact class (H). Inputs $x_1, x_2, \ldots x_n$ were propagated forward by the artificial neurons. Each input was associated with a corresponding weight, $\omega_1, \omega_2, \ldots \omega_n$. The neuron computed a weighted sum of the inputs, added a bias term, and applied an activation function to introduce nonlinearity into its output. The weighted sum and activation function were calculated as follows [41]:

$$Z_j = \sigma_j\left(\sum_{i=1}^{n} \omega_{ij} x_i + b_j\right), \tag{1}$$

where n is the number of neurons in the layer, Z is the output, σ is the activation function, and b is the bias threshold. The output summation from neurons passed through a nonlinear activation function (σ_j), named SoftMax, and it was defined as:

$$\sigma_j = \frac{e^j}{\sum_{i=1}^{n} e^{x_i}}, \tag{2}$$

To train the ANNs, the backpropagation process was used to compute the gradient of the loss function with respect to the weights of the network and update them through Adam optimization, as follows:

$$\vartheta_t = \vartheta_{t-1} - \gamma\left(\frac{m_t}{\sqrt{v_t + \epsilon}}\right), \tag{3}$$

where m_t is exponential moving average or momentum, v_t is exponential moving average or variance, ϵ is a small constant to avoid division by zero, and γ is the learning rate.

2.5. SVM

The SVM is a data-driven approach employed for classification and regression tasks with high-dimensional spaces by creating a hyperplane to distinguish the data into two classes. According to [19], the SVM has excelled with small datasets and nonlinear tasks but has underperformed on larger samples and multi-classification tasks. The objective of the SVM algorithm is to determine the optimal hyperplane in an N-dimensional space

that can efficiently separate the data points into various classes within the feature space. The dimensionality of the hyperplane depends on the number of features. Visualizing a hyperplane becomes increasingly complex with the number of features.

Initially, the SVM was designed to address binary classification problems; however, the algorithm was recently extended to handle issues with more than two classes [42]. This study employed a one-versus-one method to break down the multi-class problem into multiple binary classification tasks. This approach built $k(k-1)/2$ classifiers, where each classifier was trained using data points from two distinct classes. In a scenario involving four classes, six classifiers were constructed: $C^{12}, C^{13}, C^{14}, C^{23}, C^{24}$, and C^{34}. Each classifier consisted of two classes, assigned either +1 or -1 during training. We deduced the SVM binary method from [43] to train the classes.

2.6. Fully Convolutional Networks (FCNs)

A fully connected network (FCN) is a category of artificial neural network in which every neuron in one layer is linked to all neurons in the subsequent layer. FCNs consist of convolutional, batch normalization, pooling, and fully connected layers [44]. This article employed a fully connected network by stacking three convolutional layers with filter widths of 128, 64, and 32, with a uniform kernel filter of 3×1, succeeded by the ReLU activation function. The third convolutional layer was subjected to global average pooling, followed by a SoftMax layer for damage severity classification.

2.7. MS-1D-CNN

Lamb wave signals acquired from composite materials are inherently complex because of factors such as different damage severities, damage locations, environmental noise, and reflections from plate boundaries. To address the limitations of the traditional 1D-CNN in extracting essential features from complex signals, we proposed a multiscale-1D-CNN model, as illustrated in Figure 4, for the classification and localization of damage severity. Each input sample, with a shape of (6000, 1), was fed into three parallel convolutional blocks, with different kernel sizes (3×1, 5×1, and 7×1) arranged in increasing order. The small kernel (3×1) focuses on smaller temporal scales in the signals, such as sharp amplitude changes or small anomalies from the damage. The medium kernel (5×1) helps identify moderate reductions in amplitude due to edge reflections and material damping. The large kernel (7×1) captures the overall wave packets, identifying spatial patterns, such as significant signal variations [45–49].

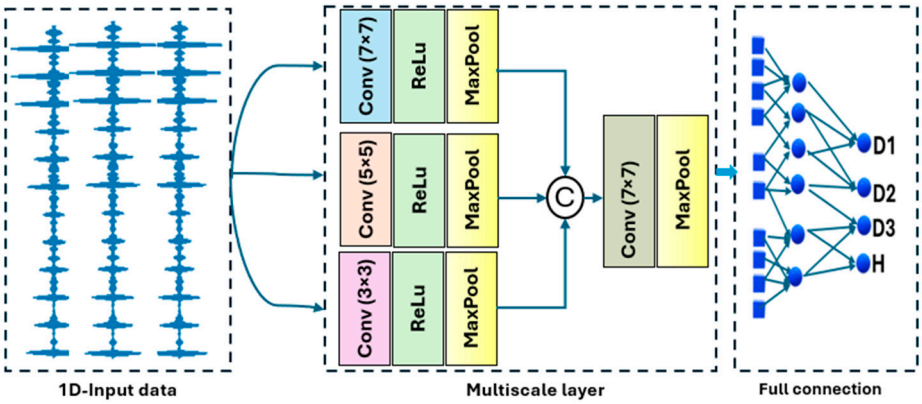


Figure 4. The architecture of the multiscale one-dimensional convolution neural network (MS-1D-CNN) model.

After each convolution operation, the ReLU activation function was applied to introduce nonlinearity into the network and enhance learning efficiency. This was followed by a

max-pooling operation to extract and retain the most significant features. The outputs from the three blocks were then concatenated to form a combined feature representation, which was subsequently passed through an additional convolutional layer and a max-pooling operation to further reduce the dimensionality. The resulting output was flattened and passed through fully connected dense layers, incorporating dropouts for regularization. Finally, the SoftMax layer classified the signal into four predefined classes: D1, D2, D3, and H. The detailed architecture of the MS-1D-CNN model for damage severity classification is presented in Table 1. The convolution process for each kernel for the one-dimensional signal was expressed as follows:

$$z_j^l = f\left(\sum_{i=M_j} z_i^{l-1} \times k_i^l + b_j^l\right), \tag{4}$$

where M_j is the index of the kernels for the multiscale operation, k_i^l is the ith convolutional kernel, b_j^l is the bias term, and z_j^l is the output feature map on the jth convolutional kernel at l layer. The nonlinear activation function f, known as ReLU, was applied to each output feature map z_j^l, and the activated output for the jth kernel was expressed as follows [45,46]:

$$b_j^l = f\left(z_j^l\right), \ for \ \ j = 1, 2, 3 \tag{5}$$

if $f(x) = ReLU(x) = \max(0, x)$, then:

$$b_j^l = \max\left(0, z_j^l\right) \tag{6}$$

Table 1. Architecture of MS-1D-CNN for damage severity classification.

Layer	Output Shape	Parameters
Input layer	(None, 6000, 1)	0
Conv1	(None, 6000, 32)	128
Conv2	(None, 6000, 64)	348
Conv3	(None, 6000, 128)	1024
Pool1	(None, 3000, 32)	0
Pool2	(None, 3000, 64)	0
Pool3	(None, 3000, 128)	0
Concatenate	(None, 3000, 224)	0
Conv4	(None, 3000, 128)	200,832
Pool4	(None, 1500, 128)	0
Flatten	(None, 192,000)	0
Dense1	(None, 512)	98,304,512
Dropout	(None, 512)	0
Dense2	(None, 4)	2052
Total parameters: 98,508,932, Trainable parameters: 98,508,932, Non-trainable parameters: 0		

Max-pooling was introduced to reduce the spatial dimensions of the feature maps while maintaining significant activation. For three distinct kernels, the max-pooling output, $p_j^l[t]$, was expressed as follows:

$$p_j^l[t] = \underset{i \in N}{max} \left\{b_j^l[t+i]\right\} \tag{7}$$

where b_j^l is the activation feature of the jth kernel and N is the pooling window size. The outputs from the max-pooling process were concatenated to obtain the output feature map of the MS-1D-CNN:

$$p_{concatenate}^l = \left[p_1^l,\ p_2^l,\ p_3^l\right] \tag{8}$$

2.8. Performance Evaluation Metrics

This study adopted various metrics, such as accuracy, precision, recall, F1-score, and confusion matrices, to assess the performance of each trained model. Accuracy is defined as the overall correctness, which indicates how correctly the test cases are classified. In binary classification, trained data are typically grouped into four categories: true positives (TP), false positives (FP), true negatives (TN), and false negatives (FN), based on the relationship between the true class and the predictive class of the model [45–47]:

$$\text{Accuracy} = \frac{\text{TP} + \text{TN}}{\text{TP} + \text{TN} + \text{FN} + \text{FP}}, \tag{9}$$

$$\text{Precision} = \frac{\text{TP}}{\text{TP} + \text{FP}}, \tag{10}$$

$$\text{Recall} = \frac{\text{TP}}{\text{TP} + \text{FN}}, \tag{11}$$

$$\text{F1} - \text{score} = \frac{2\text{TP}}{2\text{TP} + \text{FN} + \text{FP}}, \tag{12}$$

3. Damage Severity Classification

The network architectures were executed in Python (ver. 3.12) using Keras (ver. 3.7), with TensorFlow (ver. 2.78) as the backend. We used a batch size of 32 during training to mitigate overfitting. We set the epoch count to 50 for ANN, FCN, and MS-1D-CNN models. The Adam optimizer was employed to adjust the weights of the network during backpropagation, with a learning rate of 10^{-3}, with a decaying step of 10^4 and a decay factor of 0.9. The training settings chosen for the SVM were a regularization parameter $(C = 1)$ and linear kernel type.

3.1. Performance Comparison with Various Models

In this section, the classification results achieved by the trained models on the Lamb wave test dataset are presented, as described in Section 2.3. The performance of the MS-1D-CNN model is evaluated across three damage severities (D1, D2, and D3) and in a healthy state (H). To provide a comprehensive comparison, we also evaluate the performance of the most widely used approaches in SHM, specifically ANN, SVM, and FCN. These models are recognized for their reliability in SHM applications, and we adopted them as benchmarks for our MS-1D-CNN.

For damage severity D1, as seen in Table 2, MS-1D-CNN surpassed the other classifiers, achieving an accuracy of 0.94, a recall of 0.94, and an F1-score of 0.92. This signifies that the proposed model can categorize damage condition D1 with few false negatives. The FCN model achieved an accuracy of 0.92, a precision score of 0.90, a recall of 0.92, and an F1-score of 0.91. The artificial neural network (ANN) attained an accuracy of 0.82, a precision of 0.90, and a recall of 0.82. The ANN and FCN models effectively reduced false positives; however, they misclassified a greater number of D1 instances than the proposed MS-1D-CNN. The SVM exhibited suboptimal performance, attaining less than 60 accuracies across all metrics, which suggests challenges in accurately classifying the D1 class.

Table 2. Overall performance comparison for damage severity classification.

Health State	Classifier	Evaluation Metrics			
		Accuracy	**Precision**	**Recall**	**F1-Score**
D1	SVM	0.50	0.55	0.50	0.53
	ANN	0.82	0.90	0.82	0.86
	FCN	0.92	0.90	0.92	0.91
	MS-1D-CNN	0.94	0.90	0.94	0.92
D2	SVM	0.72	0.49	0.72	0.58
	ANN	0.85	0.82	0.85	0.84
	FCN	0.89	0.88	0.92	0.91
	MS-1D-CNN	0.89	0.93	0.94	0.94
D3	SVM	0.68	0.88	0.68	0.77
	ANN	0.90	0.87	0.90	0.88
	FCN	0.91	0.90	0.93	0.92
	MS-1D-CNN	0.94	0.93	0.94	0.94
H	SVM	0.74	1.00	0.74	0.85
	ANN	0.99	0.97	0.99	0.98
	FCN	0.93	1.00	0.93	0.96
	MS-1D-CNN	0.97	1.00	0.97	0.99

The MS-1D-CNN demonstrated superior performance for damage severities D2 and D3, achieving an accuracy of 0.89 for D2 and 0.94 for D3. The model achieved a precision of 0.93, with both recall and F1-score at 0.94. These results indicate our model's effectiveness in reducing both false positives and false negatives within these categories. The FCN model demonstrated a moderate result in classifying D2 and D3, attaining accuracy scores exceeding 90. However, it exhibited a relatively low precision of 0.88 for D2. The ANN and SVM models demonstrated limited effectiveness in these scenarios, with the ANN achieving the precision score of 0.82 for D2 and 0.87 for D3, alongside F1-scores of 0.84 and 0.88, respectively. The SVM encountered difficulties in classifying both D2 and D3, attaining a validation score under 0.85, with the exception of 0.88 in precision for D3. The artificial neural network (ANN) demonstrated exceptional performance in identifying the healthy state (H), achieving an accuracy of 0.99, with a precision, recall, and F1-score of 0.98, indicating a high capability to accurately identify the healthy state with minimal errors. The MS-1D-CNN demonstrated a precision of 1.00 and a recall of 0.97, indicating robust performance in differentiating between healthy and damaged states. Both the SVM and FCN attained a precision of 1.00; however, the SVM exhibited deficiencies in accuracy and recall, underscoring its limitations in classifying healthy states.

Figure 5a–d present the confusion matrix from the testing data to explain the performance of the proposed model further. The confusion matrix indicated that the MS-1D-CNN, FCN, ANN, and SVM correctly classified the tested samples with overall accuracies of 0.93, 0.91. 0.85, and 0.67, respectively. The proposed MS-1D-CNN exhibited excellent classification across all classes, as illustrated in Figure 5a. The model accurately classified classes D1, D3, and H, with only minor misclassifications. Nevertheless, the model exhibited a low accuracy of 0.88 for D2, as 0.69 of the D2 samples were inaccurately classified as D1 and 0.46 as D3. The FCN model shown in Figure 5b outperformed all the models in classifying D3, with 97.1% accuracy, while MS-1D-CNN, ANN, and SVM classified it with an accuracy of 0.94, 0.89, and 0.77, respectively. Analogous to the ANN model shown in Figure 5c, it performed poorly on the D2 class, with an accuracy of 0.76. The misclassification of D2 as D1 and D3 classes across all models may result from the resemblance in the characteristics of D2 to other damage severities, which impairs the capacity of the models to accurately

classify D2 damages. Moreover, the class imbalance could have hindered the model performance in the D2 class because of its fewer testing samples relative to other courses. SVM was the worst model, with the highest number of incorrectly classified classes, as shown in Figure 5d.

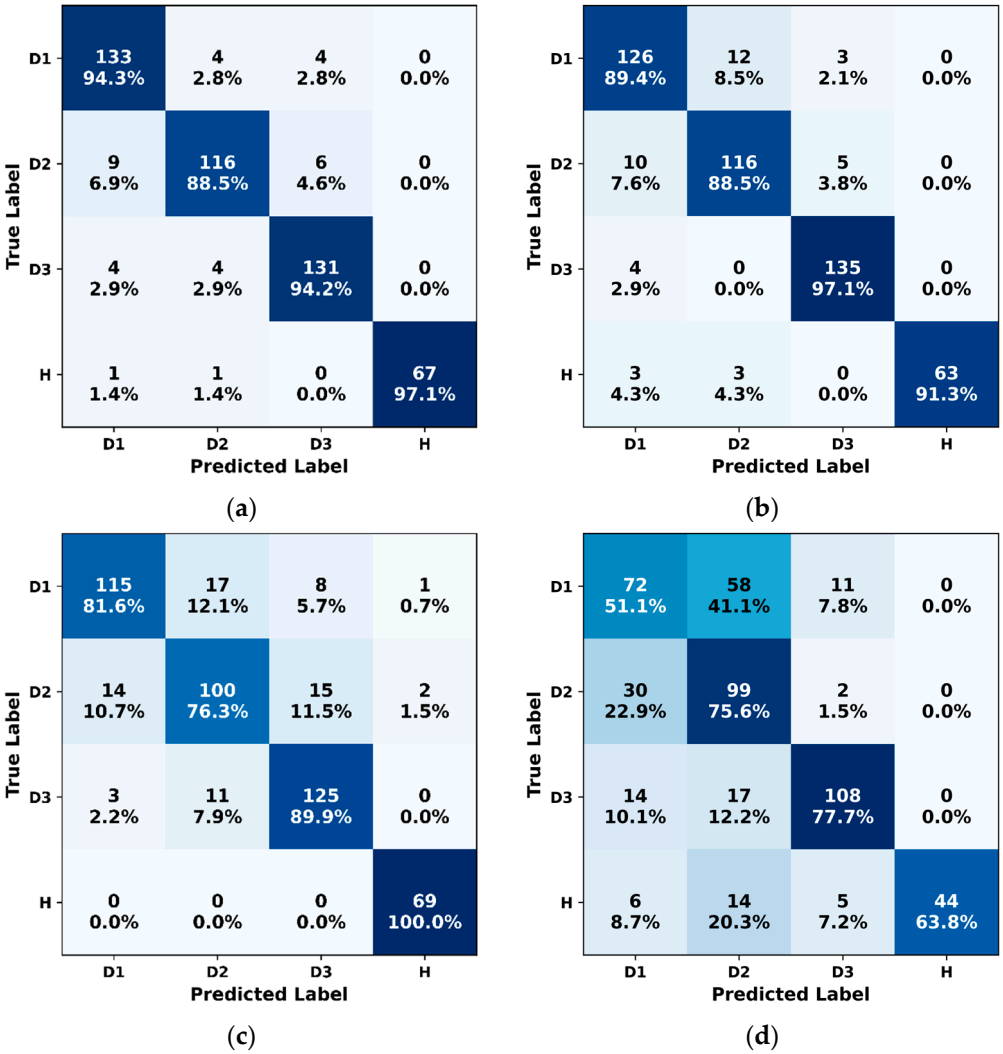


Figure 5. Confusion matrix: (**a**) MS-1D-CNN model, (**b**) FCN model, (**c**) ANN model, and (**d**) SVM model.

The performance metrics were evaluated using 5-fold cross-validation, and the findings are presented as the mean ± standard deviation for each model, as presented in Figure 6. This approach guarantees reliable and unbiased evaluation of different machine learning models tested on unseen data, including MS-1D-CNN, ANN, FCN, and SVM, across all classification tasks. The results of the 5-fold cross-validation indicated that the MS-1D-CNN outperformed the other models with the highest mean accuracy (0.92) and the smallest standard deviation (±0.006), showcasing both superior performance and exceptional stability. The FCN model showed a validation accuracy of 0.90 with a standard deviation of ±0.016. The ANN also performed well, with a mean accuracy of 0.88 (±0.012), demonstrating strong classification capability but slightly less stability than the MS-1D-CNN. In contrast, the SVM showed comparatively lower performance, with a mean accuracy of 0.69 (±0.038) and a wider variation across folds, reflecting less reliability and effectiveness in handling the classification task.

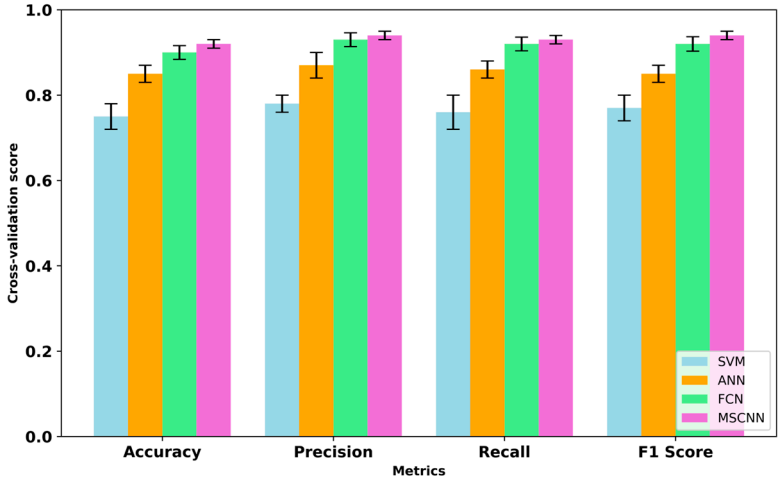


Figure 6. The performance metrics scores after 5-fold cross-validation (mean ± standard deviation) for different machine learning models.

Across all damage severity levels and the healthy state, the MS-1D-CNN consistently demonstrated the best overall performance, excelling in all metric scores. It was particularly effective at minimizing both false positives and false negatives, making it the most reliable model for detecting damages in the dataset. However, SVM consistently underperformed across all metrics, particularly accuracy and recall, making it the least effective model for this damage severity classification task.

3.2. Damage Localization

During damage localization, healthy data were excluded, and 270 damaged samples remained (90 samples per damage severity). Similar to the damage severity classification, five Gaussian noises were added to the data to improve the robustness and generalization capability of the proposed model. We increased the data 5 times, resulting in a total of 1350 damaged samples. The nine damage coordinates are shown in Figure 2b, and three types of damage were simulated using 13 g, 15 g, and 20 g for D1, D2, and D3, respectively. The architecture of the MS-1D-CNN model, as illustrated in Table 1, was slightly modified to perform the multi-regression task. For this purpose, the dense-layer output was adjusted to two units to represent the (x, y) coordinates, and no activation function was applied to the output layer. Instead of using the categorical cross-entropy as the loss function, the mean squared error (MSE) was employed, which is more appropriate for regression tasks. Additionally, the classification accuracy metrics were replaced with regression-specific metrics, including the mean absolute error (MAE) and MSE.

We evaluated the MS-1D-CNN regression model using five-fold cross-validation by dividing the dataset into five folds to ensure a balanced distribution of the target variables in each fold. Model performance was assessed using three evaluation metrics: MAE, MSE, and R^2. The proposed MS-1D-CNN model was benchmarked against other regression models, including the ANN, FCN, and SVM, to validate its effectiveness. The 5-fold cross-validation was implemented using the k-fold function from Scikit-learn, splitting the dataset into training and validation sets for each fold. The model was trained using the training set and validated using the corresponding validation set. After training, the performance metrics were computed for each fold, and the mean and standard deviation of these metrics were reported to ensure a robust evaluation. To assess the accuracy of the results across the nine locations, the error function for each model was estimated as follows [50]:

$$\varepsilon_r = \sqrt{(x_p - x_r)^2 + (y_p - y_r)^2}, \quad (13)$$

where (x_r, y_r) are the actual damage coordinates and (x_p, y_p) are the predicted damage coordinates. The effectiveness of the proposed model is illustrated in Table 3, which summarizes the performance of each model across three distinct metrics. The MS-1D-CNN demonstrated outstanding performance in localizing damage, achieving the lowest mean absolute error of 10.57 mm. This confirmed the accuracy of the model in predicting the actual location with minimal deviation. Furthermore, an MSE of 306.29 mm underscored its ability to minimize more significant prediction errors effectively. To assess the R^2 for each model, our model outperformed the remaining models, with improvements of 2.15%, 3.3%, and 6.9% for the FCN, ANN, and SVM, respectively. Table 4 presents a summary of the predicted locations and the corresponding average errors for each damage severity level for the proposed MS-1D-CNN model. The results indicated that the proposed model estimated the positions for damage severities D1 and D2 with average errors of 14.63 mm and 14.48 mm, respectively, reflecting a minor yet significant deviation from the actual coordinates. The error for D1 exceeded that of D2 marginally, with a difference of 0.15 mm. The observed variance can be attributed to factors including the slight attenuation of signals resulting from the slight mass difference between D1 (13 g) and D2 (15 g), along with potential variability in the experimental conditions. Additionally, the model encountered challenges in identifying subtle patterns in both D1 and D2 signals, which may have resulted in higher errors in some cases. Interestingly, the predicted locations for D1 and D2 did vary, and in some cases, the error for D2 was slightly higher than for D1. This variability suggests that, while the masses of D1 and D2 are close, their signal characteristics may overlap, leading to some uncertainty in their identification. The model accurately predicted the location of damage severity D3, showing a significantly smaller error of 5.14 mm compared to D1 and D2. This confirmed that a larger mass of 20 g for D3 generated stronger and distinct signals, which in turn led to clearer patterns in the signals.

Table 3. Comparison results for MS-1D-CNN, ANN, and SVM to localize damages.

Model	MAE (mm)	MSE (mm^2)	R^2 (%)
SVM	15.80	519.74	0.87
ANN	12.34	324.77	0.90
FCN	13.75	400.10	0.91
MS-1D-CNN	10.57	306.29	0.93

Table 4. Predicted locations with their corresponding errors for different damage severities for MS-1D-CNN.

Actual Location (mm)		Predicted Location for D1 (mm)		Estimated Error (mm)	Predicted Location for D2 (mm)		Estimated Error (mm)	Predicted Location for D3 (mm)		Estimated Error (mm)
x_r	y_r	x_p	y_p	ε_r	x_p	y_p	ε_r	x_p	y_p	ε_r
67	83	72.66	79.42	6.70	66.97	88.86	5.86	64.8	84.03	2.43
67	154	84.55	143.09	20.66	66.62	157.5	3.52	66.63	149.93	4.09
67	226	66.45	213.68	12.33	73.19	200.5	26.24	65.31	225.35	1.81
157	83	149.99	80.33	7.50	152.1	91.84	10.11	155.83	78.13	5.01
157	154	132.67	133.34	31.92	146.3	141.92	16.14	166.72	148.51	11.16
157	226	162.25	228.81	5.95	158.78	237.52	11.66	152.03	221.21	6.90
247	83	239.27	89.37	10.02	221.35	77.54	26.22	241.16	88.63	8.11
247	154	222.23	158.24	25.13	242.07	141.33	13.60	248.67	157.72	4.08
247	226	241.19	216.12	11.46	230.7	221.17	17.00	248.96	224.17	2.68
		Average error (mm)		14.63	Average error (mm)		14.48	Average error (mm)		5.14

Figure 5a–c present the visualization plots of the MS-1D-CNN model used for localizing damage severities, where magenta, cyan, and blue dots represent the predicted locations for the D1, D2, and D3 damage severities, respectively, and the chocolate dots at the corners represent PZTs. Poor localization is evident in Figure 7a for damage severity D1, followed by moderate localization performance for damage severity D2 in Figure 7b. D3 yielded the best results. Figure 7c shows the best results for the damage severity D3, where the predicted locations aligned closely with the actual locations. The increase in prediction accuracy from D1 to D3 indicated that the model performed well with increasing damage mass, which likely enhanced signal clarity and, consequently, the localization results.

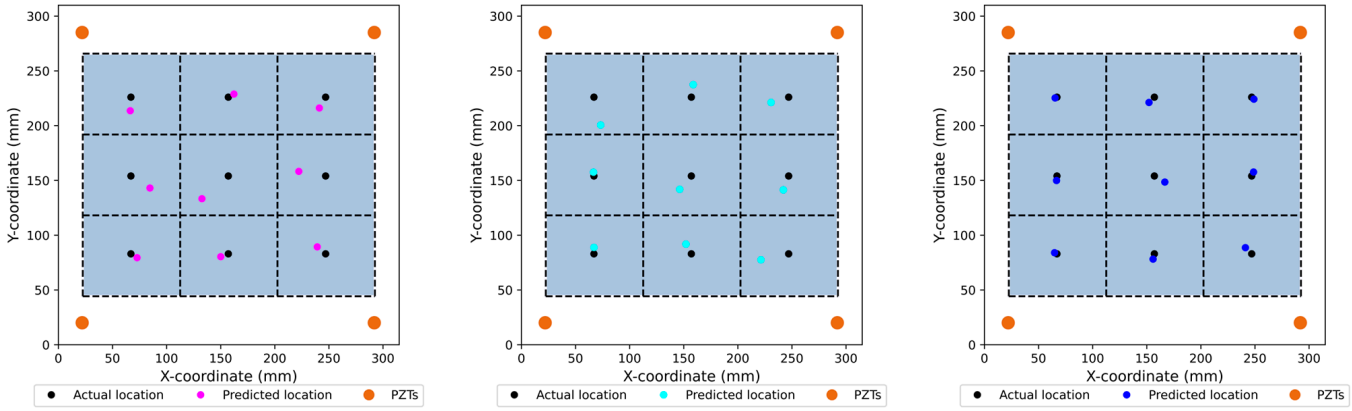


Figure 7. Actual and predicted locations for the MS-1D-CNN model: (**a**) damage severity D1, (**b**) damage severity D2, and (**c**) damage severity D3.

4. Conclusions

This study proposed and developed a MS-1D-CNN model to classify and localize the damage severity in composite plate structures. This study involved conducting a Lamb wave experiment on a composite plate using four PZT transducers to generate and capture Lamb wave signals. Five levels of Gaussian noise were added to the preprocessed data to improve the robustness of the model and to simulate real-world conditions. The trained models were evaluated using multiple metrics, including accuracy, precision, recall, and F1-score, for damage severity classification. The MAE, MSE, and the R^2 score were used for localization. The MS-1D-CNN surpassed FCN, ANN, and SVM models in damage classification, with overall test accuracies of 92.5 $\pm$ 0.006%, 90.0 $\pm$ 0.016%, 88.4 $\pm$ 0.012%, and 69.3 $\pm$ 0.038%, respectively. The proposed model had excellent performance in localizing damage severity, with a minimal average error of 5.14 mm for severity D3, followed by D2 and D1 with average errors of 14.48 mm and 14.63 mm, respectively. The proposed model surpassed FCN, ANN, and SVM in both classification and localization of damages. Nevertheless, our approach presented challenges in identifying and localizing certain minor damages, particularly D1. Consequently, future efforts will focus on enhancing the efficiency of the model for detecting minor damage.

Author Contributions: Conceptualization, J.W.S.; methodology, O.M.; writing—original draft preparation, O.M.; writing—review and editing, O.M. and J.W.S.; supervision, J.W.S. All authors have read and agreed to the published version of the manuscript.

Funding: This work was partly supported by a National Research Foundation of Korea (NRF) grant funded by the Korean Government (Ministry of Science and ICT, MSIT; RS-2023-NR076925, 50%). This work was also partly supported by the Institute of Information and Communications Technology Planning and Evaluation (IITP)—Innovative Human Resource Development for Local

Intellectualization program grant, funded by the Korean government (MSIT; IITP-2025-RS-2020-II201612, 50%).

Data Availability Statement: Data are contained within the article.

Conflicts of Interest: The authors declare no conflicts of interest.

References

1. Rajak, D.K.; Pagar, D.D.; Kumar, R.; Pruncu, C.I. Recent progress of reinforcement materials: A comprehensive overview of composite materials. *J. Mater. Res. Technol.* **2019**, *8*, 6354–6374. [CrossRef]
2. Hasan, M.; Zhao, J.; Jiang, Z. Micromanufacturing of composite materials: A review. *Int. J. Extrem. Manuf.* **2019**, *1*, 12004. [CrossRef]
3. Singh, H.; Brar, G.S.; Kumar, H.; Aggarwal, V. A review on metal matrix composite for automobile applications. *Mater. Today Proc.* **2020**, *43*, 320–325. [CrossRef]
4. Salama, A.; El-Sakhawy, M. Polysaccharides/propolis composite as promising materials with biomedical and packaging applications: A review. *Biomass Convers. Biorefinery* **2022**, *14*, 4555–4565. [CrossRef]
5. Chi, H.; He, W.; Zhao, D.; Ma, R.; Zhang, Y.; Jiang, Z. Recent progress of dielectric polymer composites for bionics. *Sci. China Mater.* **2023**, *66*, 22–34. [CrossRef]
6. Cao, H.; Ma, Y.; Wu, L.; Yu, L.; Elbadry, E.A.; Yang, W.; Huang, X.; Yan, X. Effect of fiber breakage position on the mechanical performance of unidirectional carbon fiber/epoxy composites. *Rev. Adv. Mater. Sci.* **2021**, *60*, 352–364. [CrossRef]
7. Kidangan, R.T.; Krishnamurthy, C.V.; Balasubramaniam, K. Identification of the fiber breakage orientation in carbon fiber reinforced polymer composites using induction thermography. *NDT E Int.* **2021**, *122*, 102498. [CrossRef]
8. Humer, C.; Höll, S.; Kralovec, C.; Schagerl, M. Damage identification using wave damage interaction coefficients predicted by deep neural networks. *Ultrasonics* **2022**, *124*, 106743. [CrossRef]
9. Jeon, J.Y.; Miao, Y.; Park, G.; Flynn, E. Compressive laser scanning with full steady state wavefield for structural damage detection. *Mech. Syst. Signal Process.* **2022**, *169*, 108626. [CrossRef]
10. Giannakeas, I.N.; Khodaei, Z.S.; Aliabadi, F.M.H.H. Effect of detection and localization uncertainty on damage size estimation using guided wave based SHM. *Procedia Struct. Integr.* **2024**, *52*, 655–666. [CrossRef]
11. Ullah, S.; Ijjeh, A.A.; Kudela, P. Deep learning approach for delamination identification using animation of Lamb waves. *Eng. Appl. Artif. Intell.* **2023**, *117*, 105520. [CrossRef]
12. Wang, J.; Schmitz, M.; Jacobs, L.J.; Qu, J. Deep learning-assisted locating and sizing of a coating delamination using ultrasonic guided waves. *Ultrasonics* **2024**, *141*, 107351. [CrossRef] [PubMed]
13. Ijjeh, A.A.; Kudela, P. Deep learning-based segmentation using full wavefield processing for delamination identification: A comparative study. *Mech. Syst. Signal Process.* **2022**, *168*, 108671. [CrossRef]
14. Pineda Allen, J.C.; Ng, C.T. Damage detection in composite laminates using nonlinear guided wave mixing. *Compos. Struct.* **2023**, *311*, 116805. [CrossRef]
15. Zeng, X.; Zhao, B.; Liu, X.; Yu, Y.; Guo, J.; Qing, X. Lamb wave-based damage assessment for CFRP composite structures using a CHMM-based damage localization algorithm and a damage quantitative expression. *Mech. Syst. Signal Process.* **2023**, *184*, 109750. [CrossRef]
16. Yang, Z.; Zhang, J.; Xu, H.; Yang, L.; Ma, S.; Wu, Z. Phased array system for damage detection in plate-like structures based on single Lamb wave mode extraction. *J. Aerosp. Eng.* **2023**, *36*, 04023004. [CrossRef]
17. Wang, Y.; Liao, Y.; Cui, X.; Huang, Y.; Qing, X. A heterogeneous decision voting-based transfer domain adaptation method for damage localization of CFRP composite structures. *Mech. Syst. Signal Process.* **2025**, *224*, 112015. [CrossRef]
18. Cha, Y.J.; Ali, R.; Lewis, J.; Büyük, O. Deep learning-based structural health monitoring. *Autom. Constr.* **2024**, *161*, 105328. [CrossRef]
19. Yang, Z.; Yang, H.; Tian, T.; Deng, D.; Hu, M.; Ma, J.; Gao, D.; Zhang, J.; Ma, S.; Yang, L.; et al. A review in guided-ultrasonic-wave-based structural health monitoring: From fundamental theory to machine learning techniques. *Ultrasonics* **2023**, *133*, 107014. [CrossRef] [PubMed]
20. Perfetto, D.; Rezazadeh, N.; Aversano, A.; De Luca, A.; Lamanna, G. Composite panel damage classification based on guided waves and machine learning: An experimental approach. *Appl. Sci.* **2023**, *13*, 10017. [CrossRef]
21. Jalali, S.S.; Mahzoon, M.; Mohammadi, H. Identification of damage properties of glass/epoxy laminates using machine learning models. *Int. J. Impact Eng.* **2023**, *177*, 104510. [CrossRef]
22. Dabetwar, S.; Ekwaro-Osire, S.; Dias, J.P. Damage classification of composites based on analysis of Lamb wave signals using machine learning. *ASCE-ASME J. Risk Uncertain. Eng. Syst. Part B Mech. Eng.* **2021**, *7*, 011002. [CrossRef]

23. Viotti, I.D.; Gomes, G.F. Delamination identification in sandwich composite structures using machine learning techniques. *Comput. Struct.* **2023**, *280*, 106990. [CrossRef]
24. Lim, D.K.; Mustapha, K.B.; Pagwiwoko, C.P. Delamination detection in composite plates using random forests. *Compos. Struct.* **2021**, *278*, 114676. [CrossRef]
25. Rajeswari, D.; Khalaf, O.I.; Srinivasan, R.; Pushpalatha, M.; Hamam, H. Structural health monitoring of aircraft through prediction of delamination using machine learning. *PeerJ Comput. Sci.* **2024**, *10*, e1955. [CrossRef]
26. Gao, Y.; Sun, L.; Song, R.; Peng, C.; Wu, X.; Wei, J.; Jiang, M.; Sui, Q.; Zhang, L. Damage localization in composite structures based on Lamb wave and modular artificial neural network. *Sens. Actuators Phys.* **2024**, *377*, 115644. [CrossRef]
27. Migot, A.; Saaudi, A.; Giurgiutiu, V. Delamination depth detection in composite plates using the Lamb wave technique based on convolutional neural networks. *Sensors* **2024**, *24*, 3118. [CrossRef]
28. Lee, I.Y.; Jang, J.; Bin Park, Y. Advanced structural health monitoring in carbon fiber-reinforced plastic using real-time self-sensing data and convolutional neural network architectures. *Mater. Des.* **2022**, *224*, 111348. [CrossRef]
29. Rosafalco, L.; Manzoni, A.; Mariani, S.; Corigliano, A. Fully convolutional networks for structural health monitoring through multivariate time series classification. *Adv. Model. Simul. Eng. Sci.* **2020**, *7*, 38. [CrossRef]
30. Parziale, M.; Lomazzi, L.; Rastin, Z.; Giglio, M.; Cadini, F. Unsupervised damage localization in composite plates using Lamb waves and conditional generative adversarial networks. *Procedia Struct. Integr.* **2024**, *52*, 551–559. [CrossRef]
31. Khan, A.; Kim, H.S. Damage assessment of laminated composites using unsupervised autonomous features. *J. Thermoplast. Compos. Mater.* **2024**, *37*, 2123–2148. [CrossRef]
32. Sawant, S.; Sethi, A.; Banerjee, S.; Tallur, S. Unsupervised learning framework for temperature compensated damage identification and localization in ultrasonic guided wave SHM with transfer learning. *Ultrasonics* **2023**, *130*, 106931. [CrossRef] [PubMed]
33. Lomazzi, L.; Junges, R.; Giglio, M.; Cadini, F. Unsupervised data-driven method for damage localization using guided waves. *Mech. Syst. Signal Process.* **2024**, *208*, 111038. [CrossRef]
34. Sattarifar, A.; Nestorović, T. Damage localization and characterization using one-dimensional convolutional neural network and a sparse network of transducers. *Eng. Appl. Artif. Intell.* **2022**, *115*, 105273. [CrossRef]
35. Zong, S.; Wang, S.; Luo, Z.; Wu, X.; Zhang, H.; Ni, Z. Robust damage detection and localization under complex environmental conditions using singular value decomposition-based feature extraction and one-dimensional convolutional neural network. *Chin. J. Mech. Eng.* **2023**, *36*, 61. [CrossRef]
36. Fu, L.; Zhang, L.; Tao, J. An improved deep convolutional neural network with multiscale convolution kernels for fault diagnosis of rolling bearing. *IOP Conf. Ser. Mater. Sci. Eng.* **2021**, *1043*, 052021. [CrossRef]
37. Li, F.; Wang, L.; Wang, D.; Wu, J.; Zhao, H. An adaptive multiscale fully convolutional network for bearing fault diagnosis under noisy environments. *Measurement* **2023**, *216*, 112993. [CrossRef]
38. Liao, Y.; Huang, Y.; Wang, Y.; Wu, M.; Zhang, F.; Qing, X. Complex CFRP damage detection with dual multiscale 1DCNNs and self-selective fusion technique of guided waves. *Compos. Struct.* **2024**, *335*, 117993. [CrossRef]
39. Song, R.; Sun, L.; Gao, Y.; Peng, C.; Wu, X.; Lv, S.; Wei, J.; Jiang, M. Global-local feature cross-fusion network for ultrasonic guided wave-based damage localization in composite structures. *Sens. Actuators Phys.* **2023**, *362*, 114659. [CrossRef]
40. Khurshid, H.; Mohammed, B.S.; Bheel, N.; Cahyadi, W.A.; Mukhtar, H. Study of factors affecting the magnetic sensing capability of shape memory alloys for non-destructive evaluation of cracks in concrete: Using response surface methodology (RSM) and artificial neural network (ANN) approaches. *Heliyon* **2024**, *10*, e35772. [CrossRef]
41. Yang, L.; Zhao, J.; Zhao, J.; Ji, H.; Qiu, J.; Wu, W.; Yang, P. Local wavenumber estimation for small damages based on artificial neural network. *NDT E Int.* **2023**, *138*, 102866. [CrossRef]
42. Santosa, B. Multiclass Classification with cross entropy-support vector machines. *Procedia Comput. Sci.* **2015**, *72*, 345–352. [CrossRef]
43. Nelon, C.M. Detection of delaminations in carbon fiber reinforced polymers embedded with Terfenol-D particles using machine learning. Ph.D. Thesis, Clemson University, Clemson, CA, USA, 2020.
44. Usmankhujaev, S.; Ibrokhimov, B.; Baydadaev, S.; Kwon, J. Time series classification with inception FCN. *Sensors* **2021**, *22*, 157. [CrossRef] [PubMed]
45. Song, Y.; Du, J.; Li, S.; Long, Y.; Liang, D.; Liu, Y.; Wang, Y. Multi-scale feature fusion convolutional neural networks for fault diagnosis of electromechanical actuator. *Appl. Sci.* **2023**, *13*, 8689. [CrossRef]
46. Wang, X.; Zhang, C.; Zhang, S. Multiscale convolutional neural networks with attention for plant species recognition. *Comput. Intell. Neurosci.* **2021**, *2021*, 5529905. [CrossRef]
47. Roy, A.M. An efficient multi-scale CNN model with intrinsic feature integration for motor imagery EEG subject classification in brain-machine interfaces. *Biomed. Signal Process. Control.* **2022**, *74*, 103496. [CrossRef]
48. Kim, G.; Park, Y.M.; Yoon, H.J.; Choi, J. A multi-kernel and multi-scale learning based deep ensemble model for predicting recurrence of non-small cell lung cancer. *PeerJ Comput. Sci* **2023**, *9*, e1311. [CrossRef] [PubMed]

49. Azad, M.M.; Raouf, I.; Sohail, M.; Kim, H.S. Structural health monitoring of laminated composites using lightweight transfer learning. *Machines* **2024**, *12*, 589. [CrossRef]
50. Kalimullah, N.M.M.M.; Shelke, A.; Habib, A. A probabilistic framework for source localization in anisotropic composite using transfer learning based multi-fidelity physics informed neural network (mfPINN). *Mech. Syst. Signal Process.* **2023**, *197*, 110360. [CrossRef]

Disclaimer/Publisher's Note: The statements, opinions and data contained in all publications are solely those of the individual author(s) and contributor(s) and not of MDPI and/or the editor(s). MDPI and/or the editor(s) disclaim responsibility for any injury to people or property resulting from any ideas, methods, instructions or products referred to in the content.